On the possibility to utilize a PCO Edge 4.2 bi scientific CMOS imager for extended ultra violet and soft X-ray photon detection

R.H. Menk,[a,b,d] **F. Arfelli,**[b,c] **M. Cautero,**[c,*] **G. Cautero,**[a,b] **M. Di Fraia,**[a] **M. Coreno,**[e,f] **F. Galdenzi**[f] **and W. Tutsch**[g]

[a] *ELETTRA Sincrotrone Trieste, Strada Statale 14, km 163.5, 34 149 Trieste, Italy*
[b] *Istituto Nazionale di Fisica Nucleare section of Trieste, via A. Valerio 2, 34 127 Trieste, Italy*
[c] *Department of Physics, University of Trieste, via A. Valerio 2, 34 127 Trieste, Italy*
[d] *Department of Medical Imaging, University of Saskatchewan, SK S7N 5A2, Saskatoon, Canada*
[e] *Consiglio Nazionale delle Ricerche, CNR-ISM, LD2 Unit, Strada Statale 14, km 163.5, 34 149 Trieste, Italy*
[f] *Istituto Nazionale di Fisica Nucleare, Laboratori Nazionali di Frascati, 00 044 Frascati, Italy*
[g] *PCO AG, Donaupark 11, 93 309 Kelheim, Germany*

E-mail: marco.cautero.96@elettra.eu

Abstract: A state of the art commercial detector, a PCO Edge 4.2 bi based on a back illuminated sCMOS sensor developed for applications in the visible light/ultra violet regime has been adapted for ultra-high vacuum operations and has been characterized using soft X-ray in the energy range from 30 eV to 1000 eV. The imager features 2048 × 2048 pixel with a pixel size of 6.5 µm × 6.5 µm and allows full frame acquisitions at 48 Hz with a dynamic range of 88 dB at a noise level of 1.9 e^-. Spatial resolution and quantum efficiency have been elucidated in the aforementioned energy range at a soft X-ray beam line at Elettra Sincrotrone Trieste. The handiness of the camera as well as

*Corresponding author.

1 Introduction

Photon science utilizing extended ultra violet (EUV) to soft X-ray photons generated by state of the art synchrotrons and FEL sources imposes an urgent need for suitable photon imaging detectors [1]. Similar to the medium to hard X-ray photon detection range [2] requirements on such EUV detectors include high (detective) quantum efficiency, high frame rates, very large dynamic range, single-photon sensitivity with low probability of false positives, small pixel pitch and (multi)- megapixels. A number of soft X-ray detectors share some, but most of the time, not all of these properties. To mention are back illuminated CCDs [3], PNCCDs [4] and to a certain extent soft X-ray silicon drift detectors [5] or integrating hybrid pixel detectors [6]. Owing to their unique features back illuminated scientific CMOS (sCMOS) imagers can be tailored to satisfy the aforementioned requirements [7]. Such application driven detector development is a sensible, albeit time consuming approach allowing to take full advantage of the luminosity improvements that free electron lasers (FELs) and diffraction-limited synchrotron rings (SRs) can provide. Conversely, the aforementioned requirements for soft X-ray detectors can be found in few state of the art commercial detectors based on sCMOS, which have been recently developed for different applications mainly in the visible light regime. In particular back thinned sCMOS sensors are well suited for experiments exploiting the water window (between 282 eV and 533 eV) and transition metal L-edges, a target photon energy range, which implies vacuum operations. Applying some modifications, in particular ultra-high vacuum (UHV) compatibleness, these commercial devices can be used for EUV and soft X-ray applications as demonstrated for instance in [8, 9].

In the following we describe the adaption of the PCO Edge 4.2 bi for soft X-ray imaging in the energy range from 35 eV–2000 eV and demonstrate preliminary results obtained with soft X-rays.

2 Materials and methods

2.1 The soft X-ray imager

The PCO Edge is built around the GSENSE2020BSI-APM-NUN PulSar back thinned single gain sCMOS sensor [10], which has been designed by Gpixel (https://www.gpixel.com) and has been processed by Tower Semiconductor (https://towersemi.com). The sensor comprises 2048 × 2048 pixels with a pixel size of 6.5 µm × 6.5 µm, which translates into an active area of 13.3 mm × 13.3 mm. With its six-transistor (6T) pixel architecture possessing also a global reset function, an intrinsic readout noise of $1.6e^-$ (rms) and a full well capacity of 55000 can be achieved. In addition utilizing correlated multiple sampling (CMS), the read noise can be further reduced to 1.2 e^- using two CMS operations. When operated in an 11 bit high dynamic range (HDR) mode the sensor's intrinsic maximum frame rate is in principle 74 frames per second (fps). Integrated into the PCO Edge 4.2 bi a full well capacity of $48000e^-$ and a readout noise of 1.9 e^- are obtained, which translates in a typical dynamic range of 88 dB. The integration time can be adjusted between 10 µs–2 seconds. Using its USB 3.1 data interface the maximum frame rate is given by 48 frames per second (fps) for the full frame while it can reach for instance 520 fps for a region of interest readout of 2048 × 128 pixels. In addition, a total of 4 trigger signals are provided to synchronize image acquisitions. Vacuum compatibility has been obtained by sealing the carrier board of the sensor (figure 1(a)), which constitutes the barrier between vacuum and normal atmosphere. In this fashion it is possible to keep the entire readout and trigger electronics in air. At the moment a KF flange based interface plate comprising Viton sealing rings is utilized to attach the sensor including its Peltier cooler to the experimental vacuum chamber (figure 1(b)) while the entire read out is kept in normal atmosphere. As expected for a Viton ring based sealing a leak test rate of 6.79×10^{-9} mbar/s He at 1.1×10^{-2} mbar has been obtained, which allowed us to operate the experiments at 10^{-7} mbar.

2.2 Beamline setup and experimental methods

Soft X-ray imaging capabilities of the PCO have been assessed at the circular polarized CiPo beam line at Elettra Sincrotrone Trieste [11]. CiPo provides a synchrotron radiation beam of variable polarization (circular to linear, not used though), which is tuneable in a very broad range of photon energies from 5 eV to 900 eV. The photon beam is produced by an electromagnetic elliptical Wiggler and is dispersed by means of two collinear monochromators, a normal incidence monochromator and a spherical grating monochromator (SGM), that alternatively provide two beams in the UV-VUV (5 eV–40 eV) and soft X-rays (40 eV–900 eV), respectively. Owing to its Peltier cooler the PCO Edge 4.2 bi was operated at a temperature of −20°C and was bolted to a four way cross equipped with a linear UHV translator holding a calibrated photodiode (AXUV from IDR) [12] and a slanted full absorbing edge, which could be moved into and out of the stationary synchrotron radiation. The cross was attached to an upstream, custom made UHV chamber, which accommodated a remote controlled hexapod carrying two pin holes (diameter of 800 µm and 30 µm)

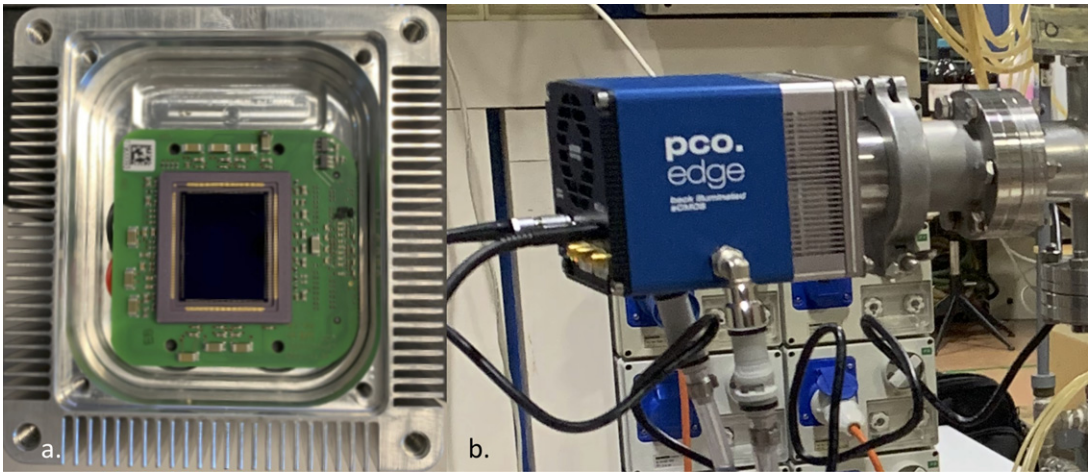

Figure 1. (a) Front view on the carrier board comprising the PulSar sensor. (b) The PCO attached to an experimental chamber utilizing the KF flange interface plate.

and which was placed 50 cm downstream of the focus of the X-rays (figure 2). Together with the AXUV the former was utilized during the estimation of the quantum efficiency while the latter allowed to generate Airy ring pattern [13], which allowed us to quantitatively estimate the contamination of the third harmonics transmitted simultaneously with the fundamental by the monochromators. The size of the beam at this position was approximately 1.5×3 mm^2, the distance between pinholes and AXUV/slanted edge was 75 cm and the distance AXUV/sensor was 25 cm.

2.3 Airy ring pattern

As pointed out above the 30 µm pin hole (Airy disk) allows to estimate the third harmonics' contamination of the fundamental, since the periodicity of the created ring pattern is coupled through

$$I(\theta) = I_0 \cdot \left[\frac{2 \cdot J_1(x)}{x}\right]^2; \qquad x = k \cdot a \cdot \sin(\theta) = \frac{2 \cdot \pi}{\lambda} \cdot \frac{q}{R} \tag{2.1}$$

to the wavelength λ of the X-rays, thus to their energy. Here I_0 is the maximum intensity of the pattern at the Airy disc centre, J_1 is the Bessel function of the first kind of order one, k is the wavenumber, a is the radius of the aperture, and θ is the angle of observation, i.e. the angle between the axis of the circular aperture and the line between aperture centre and observation point. Moreover, q is the radial distance from the observation point to the optical axis and R is its distance to the aperture. For almost all the photon energies being used for the determination of the quantum efficiency an Airy pattern has been acquired to estimate the fraction of the third harmonics and subsequently its leverage on the measured QE_m.

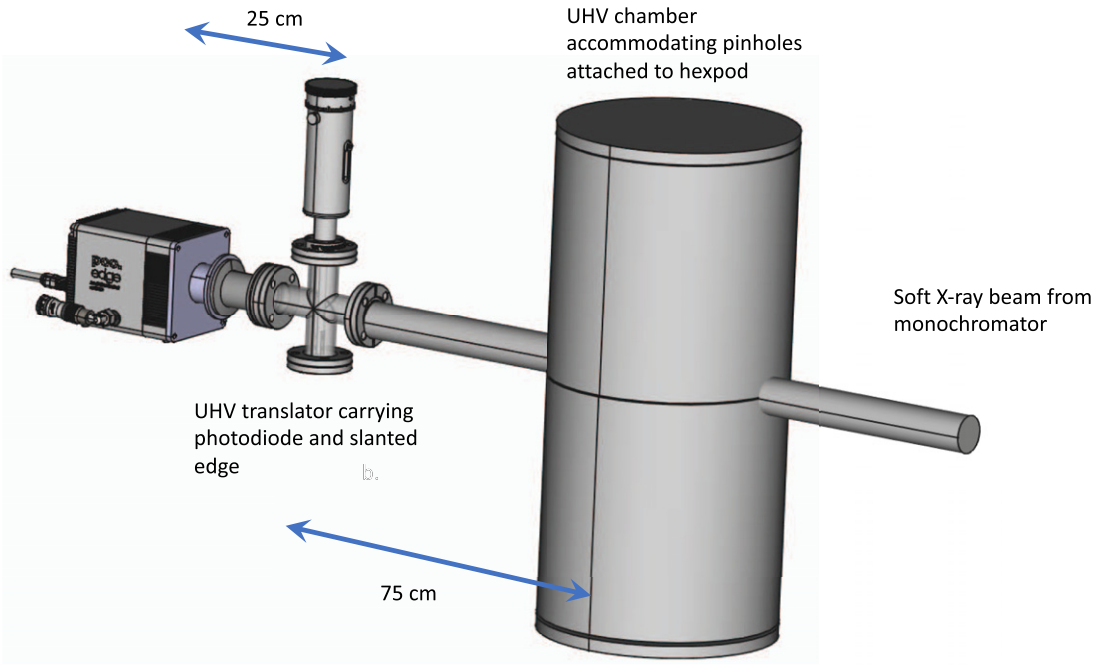

Figure 2. Experimental set up at the CiPo beamline (not in scale).

2.4 Quantum efficiency

To experimentally determine the quantum efficiency (QE_m) of the PCO Edge 4.2 bi versus the photon energy E_γ a similar procedure as described in [8] has been applied. In brief: the incidence photon flux through the 800 µm pin hole has been measured for a specific photon energy E_γ with the calibrated AXUV photodiode and has been compared to the numbers of charge carriers and subsequently photons seen by the sCMOS sensor. A conversion factor $\kappa = 0.7e^-$/ADU (analog to digital units) has to be applied to the PCO Edge offset corrected digital data to obtain the number of charge carriers, while the calibration indicated in [12] for the AXUV was used to determine the incident photon flux. It is noteworthy that the theoretical QE_{th} is a parametric function of the photon energy E_γ which can be expressed in terms of

$$QE_{th}\left(E_\gamma\right) = F\left\{\frac{\mu_i\left(E_\gamma\right)}{\rho_i}\right\} = \mathrm{e}^{-\sum_{i=1}^{N}\frac{\mu_i(E_\gamma)}{\rho_i}\cdot\rho_i\cdot x_i}\cdot\left(1-\mathrm{e}^{-\frac{\mu_{Si}(E_\gamma)}{\rho_{Si}}\cdot\rho_{Si}\cdot x_{Si}}\right) \tag{2.2}$$

where $\frac{\mu_i(E_\gamma)}{\rho_i}\cdot x_i$ is the energy dependent mass absorption coefficient of i^{th} passivation of the entrance window (or contamination layer on the latter) possessing a thickness of x_i and a density ρ_i and the second factor in the parenthesis represents the absorption of photons in the epi layer of the back-thinned sCMOS sensor with the thickness x_{Si} and the density ρ_{Si}. With the knowledge of the mass absorption coefficients taken from [14] for M different energies E_γ^j, a least square fitting procedure minimizing χ^2 with

$$\chi^2 = \frac{\sum_{j=1}^{M}\left(QE_m\left(E_\gamma^j\right. - QE_{th}\left(E_\gamma^j\right.\right)^2}{M-1} \tag{2.3}$$

allows the quantitative assessment of the (initially unknown) layer thicknesses x_i and x_{Si} in equation (2.2), respectively.

2.5 Spatial resolution

As discussed above a fully absorbing slanted edge has been utilized to investigate the spatial resolution of the sCMOS image. The slanted-edge method is specified in ISO Standard 12233 and measures the modulation transfer function (MTF), which is the modulus of the Fourier transform of the point spread function. In particular the MTF describes the magnitude response of an imaging sensor to different spatial frequencies, thus evaluating the ability of the imaging system in reproducing fine details. Utilizing a slanted edge for MTF measurements requires a linear and shift invariant imaging system and furthermore an object possessing spatial frequency components with phases that are random and uniformly distributed. This is achieved by analyzing an image of a slightly slanted fully absorbing knife-edge target. Due to the design of the aforementioned KF interface plate the minimal distance between the slanted edge and the sCMOS was 25 cm, which together with the high degree of spatial coherence of the X-ray source resulted in the observation of phase contrast effects in the edge enhancement regime. For the evaluation of the MTF the Fiji [16] software package was used, in particular the SE MTF plug-in, which can be found at https://imagej.nih.gov/ij/plugins/se-mtf/index.html).

3 Results and discussion

3.1 Airy pattern at 50 eV

As an example the measured Airy ring pattern acquired at a photon energy of 50 eV is depicted in the left panel of figure 3. Of note is that the left hand side part of the ring pattern has been obscured by the experimental chamber. Therefore the radial integration, which has been performed utilizing the radial profile plug-in of Fiji [16] was conducted only over an total angle range of 270°. The result is shown as black solid line in the right panel of figure 3 together with the theoretical expectation (blue solid line) coinciding in terms of the periodicity, which indicates a neglectable contamination (in this case <0.3%) of the third harmonics.

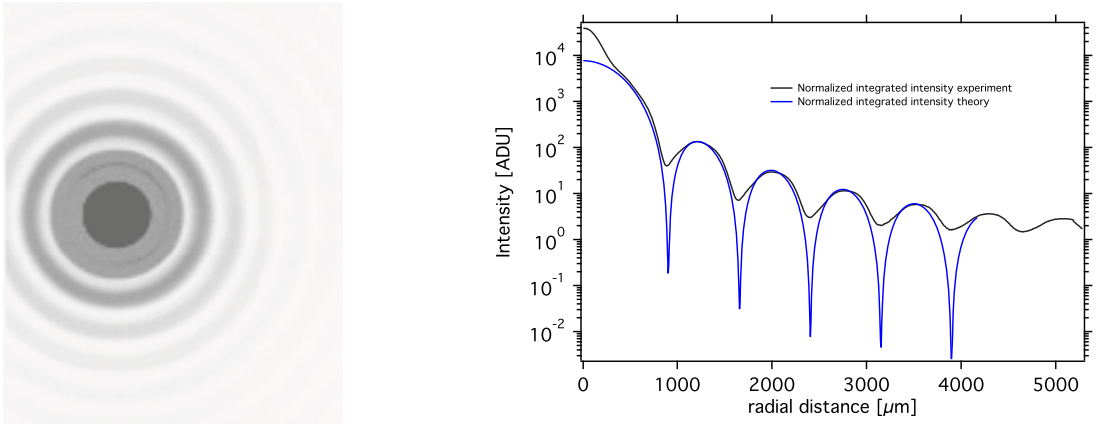

Figure 3. Left panel: Airy ring pattern acquired with 50 eV photons (black for high photon intensity and white for low photon intensity). Right panel: radial integrated Airy ring pattern (black solid line) and comparison with the theoretical prediction for the experimental conditions (blue solid line).

The intensity mismatch up to 300 µm radial distance is due to the fact, that the zero order is weighted differently during the radial integration than that of the outer rings.

3.2 Quantum efficiency in the energy range between 30 eV and 1000 eV

The measured quantum efficiency (QE_m) is depicted as blue triangles in figure 4 while the results of the least square fitting are represented by the black solid line. The indicated error bars are given by the square root of the final thus smallest χ^2 (equation (2.3)) of the least square fit, which was 0.023. Best agreement between the theoretical and experimental data has been achieved using four passivation layers in equation (2.2), assuming in particular SiO_2, an insensitive Si layer, atomic C, and fatty acid/oleate ($C_{18}H_{34}O_2$). The two latter have been initially added due to the appearance of a distinct C-edge at 284.2 eV in the experimental data and due to the well-known occurrence of C in the UHV of the CiPo beam line. Since the sCMOS sensor possesses the lowest temperature in the entire vacuum system, accumulation of atomic and organic C compounds on the sensor's surface is unavoidable resulting in the observed C edge.

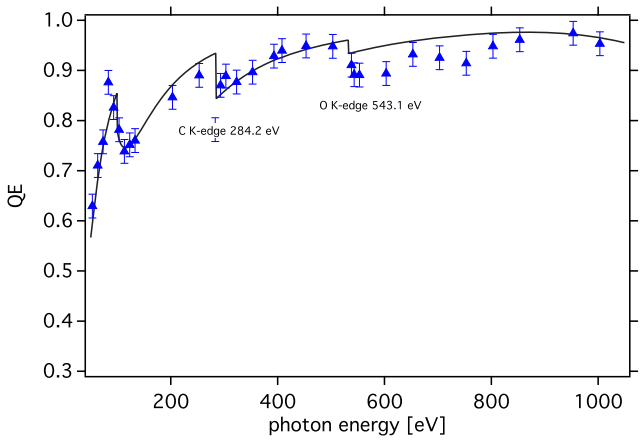

Figure 4. Measured quantum efficiency (blue triangles) versus the photon energy. The black solid line shows the result of the least square fitting.

Subsequent to the back-thinning process the doping profile of the epi layer is altered especially in the vicinity of the cleared backside, resulting in an insensitive Si layer. To the best of our knowledge no surface treatment such as δ-doping or laser annealing has been conducted on the GSENSE2020BSI-APM-NUN PulSar sensor subsequent back-thinning therefore such assumption of the existence of an insensitive Si layer is justified. Moreover, the occurrence of an oxygen edge at 543.1 eV suggest the existence of a SiO_2 passivation. The results from the least square fitting forecasts a layer thickness of 0.5 ±0.1 nm of atomic C, 12.3 ± 0.4 nm fatty acid, a 0.9 ± 0.2 nm insensitive Si layer and 9.9 ±0.1 nm SiO_2 passivation, while an Si epi layer of 10.3 ±0.2 µm is found. The latter two results coincide with the manufacturer's (Gpixel) data.

3.3 Spatial resolution

Depicted in figure 5 is the image of the slanted edge acquired using 400 eV photons. As mentioned above, due to the high degree of coherence and the elevated edge to sensor distance the principle phase contrast fringe is visible close to the edge.

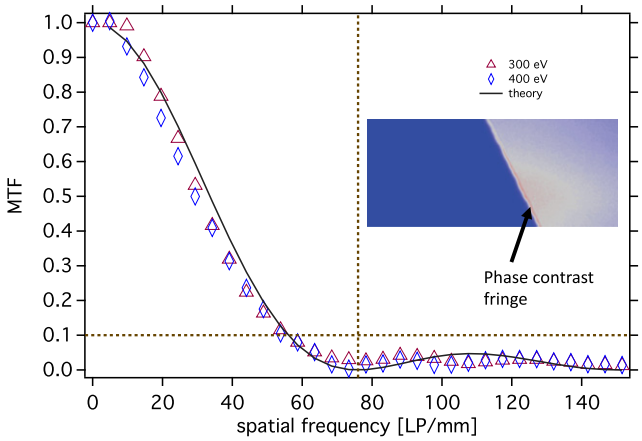

Figure 5. Image of the slanted edge acquired at a photon energy of 400 eV and resulting the MTFs for 400 eV and 300 eV, respectively.

Moreover, it is noticeable that the knife edge is not ideal but possesses some modulation along the blade, which impacts the low spatial frequency behavior of the MTFs recorded at 300 eV (red triangles) and 400 eV (blue diamonds). Also shown in figure 5 is the theoretical progression of the MTF (black solid line) for a pixel size of 6.5 µm, a sinc function when assuming a box like point spread function. As expected the zero crossing of the measured MTFs is at approximately 77 LP/mm, while the 10% of the normalized MTF (a common metrics for the spatial resolution) is reached approximately at 55 LP/mm.

4 Conclusion and outlook

Here we presented first measurements with a modified soft X-ray PCO Edge 4.2 bi carried out at the CiPo beamline at Elettra Sincrotrone Trieste showing a very high quantum efficiency, which is greater than 60% in the energy range between 30 eV and 200 eV and greater than 80% for energies between 200 eV and 1000 eV. This is somewhat higher than the QE measured for Gpixel's GSENSE400BSI-TVISB and the GSENSE400BSI-GP sensors, which have been presented in [9] and is due to the different chip design. Airy ring pattern have been utilized to determine the fraction of the third harmonics that is transmitted simultaneously with the fundamental through the monochromator system. From the comparison to the theoretical model it turns out that the harmonics contamination is less than 0.3% therefore no harmonics correction has been applied to the experimental QE measurements. Likewise the low harmonics content shows little impact on the spatial resolution, which is 55 LP/mm at the 10% level of the normalized MTF and follows

almost the sinc function of an ideal imaging system featuring a box like point spread function. During the QE measurements the SiO_2 passivation was exposed to an (estimated) entrance dose of about 7000 Gy at an estimated dose rate of 40 Gy/s resulting in surface damage due to the ionizing radiation. Like in the silicon bulk, X-rays produce electron-hole pairs in the SiO_2. Whereas the mobility of electrons is sufficiently high so that they can escape to a nearby electrode, holes are trapped, which results in a positive charge layer and interface traps at the Si-SiO_2 interface [15] increasing the leakage current. Due to the wiring of the backend electronics the increase in leakage current results in a reduction of the digital units in the pedestal image. In our specific case we observed a reduction of about 0.7% and subsequently an increase of the noise by 3.2%. More quantitative investigations on radiation damage are currently carried out and will be discussed in future. Presently several beam time campaigns are conducted to elucidate the detective quantum efficiency and the energy resolution for single photon events of the camera, but also here data mining is still ongoing. Moreover, some scientific imaging applications at Elettra's soft X-ray microscope TwinMic and at the coherent diffraction imaging beamline DiProi at the Fermi free electron laser have been carried out providing very promising preliminary results. During these experiments the handiness of the PCO Edge 4.2 bi and its easy integration into the beamline control through a Python library package has been highly appreciated by the experimentalists. From these preliminary experiments it can be concluded that the PCO Edge 4.2 bi prototype discussed here is well suited for soft X-ray applications at synchrotrons and free electron lasers.

Acknowledgments

The authors are grateful to PCO for providing a modified PCO Edge 4.2 bi for the experiments described here. Moreover, we like to acknowledge the contributions of T. Prudil and N. Lindner, both with PCO and of M. Barnaba from Elettra for the UHV adaption of the camera. We also like to thank L. Rumiz and R. Giovanoni for their help during the vacuum tests and W. Avallone and G. Lautizi for their help throughout data taking at CiPo. Eventually we express our gratitude to Yuxia Wu from Gpixel to share information on passivation and epi layer thickness and N. Zema and F. Zuccaro for the beamline support.

References

[1] T. Hatsui and H. Graafsma, *X-ray imaging detectors for synchrotron and XFEL sources, Int. Union Crystallogr.* **2** (2015) 371.

[2] H. Graafsma, J. Becker and S.M. Gruner, *Integrating hybrid area detectors for storage ring and free-electron laser applications, Int. Union Crystallogr.* (2020) 1225 [ISBN : 978-3-030-23200-9].

[3] P. Denes, D. Doering, H.A. Padmore, J.P. Walder and J. Weizeorick, *A fast, direct X-ray detection charge-coupled device, Rev. Sci. Instrum.* **8** (2009) 80.

[4] L. Strüder et al., *Large-format, high-speed, X-ray pnCCDs combined with electron and ion imaging spectrometers in a multipurpose chamber for experiments at 4th generation light sources*, *Nucl. Instrum. Meth. A* **614** (2010) 483.

[5] I. Carlomagno et al., *Trace-element XAFS sensitivity: a stress test for a new XRF multi-detector*, *J. Synchrotron Radiat.* **28** (2021) 1811.

[6] S. Cartier et al., *Micrometer-resolution imaging using MÖNCH: towards G2-less grating interferometry*, *J. Synchrotron Radiat.* **6** (2016) 1462.

[7] A. Marras et al., *Characterization of the Percival detector with soft X-rays*, *J. Synchrotron Radiat.* **28** (2020) 131.

[8] K. Desjardins et al., *Characterization of a back-illuminated CMOS camera for soft X-ray coherent scattering*, *AIP Conf. Proc.* **2054** (2019) 060066.

[9] K. Desjardins et al., *Backside-illuminated scientific CMOS detector for soft X-ray resonant scattering and ptychography*, *J. Synchrotron Radiat.* **27** (2020) 1.

[10] C. Ma, Y. Liu, J. Li, Q. Zhou, Y. Chang and X. Wang, *A 4MP high-dynamic-range, low-noise CMOS image sensor*, *SPIE Int. Society Optics Photonics* **9403** (2015) 26.

[11] D. Desiderio et al., *The Elettra circular polarization beamline and electromagnetic elliptical wiggler insertion device*, *Synchrotron Radiat. News* **12** (1999) 34.

[12] M. Bernert et al., *Application of AXUV diode detectors at ASDEX Upgrade*, *Rev. Sci. Instrum.* **85** (2014) 033503.

[13] G.B. Airy, *On the diffraction of an object-glass with circular aperture*, *Trans. Cambridge Philos. Soc.* **5** (1835) 283–289.

[14] M.J. Berger et al., XCOM: photon cross sections database, *NIST Standard Reference Database 8 (XGAM)*, (2010).

[15] C.W. Fabjan, Detectors for particles and radiation, *Particle Physics Reference Library*, Vol. 2, Springer (2020) [ISBN: 978-3-030-35320-9].

[16] J. Schindelin et al., *Fiji: an open-source platform for biological-image analysis*, *Nat. Methods* **9** (2012) 676.